Density distributions of ^{11}Li deduced from reaction cross-section measurements

T. Moriguchi,[1,*] A. Ozawa,[1,†] S. Ishimoto,[2] Y. Abe,[1] M. Fukuda,[3] I. Hachiuma,[4] Y. Ishibashi,[1] Y. Ito,[1] T. Kuboki,[4] M. Lantz,[5,‡] D. Nagae,[1] K. Namihira,[4] D. Nishimura,[3,§] T. Ohtsubo,[6] H. Ooishi,[1] T. Suda,[5,∥] H. Suzuki,[1,¶] T. Suzuki,[4] M. Takechi,[5,**] K. Tanaka,[5] and T. Yamaguchi[4]

[1]*Institute of Physics, University of Tsukuba, Tsukuba, Ibaraki 305-8571, Japan*
[2]*High Energy Accelerator Research Organization (KEK), Tsukuba, Ibaraki 305-0801, Japan*
[3]*Department of Physics, Osaka University, Osaka 560-0043, Japan*
[4]*Department of Physics, Saitama University, Saitama 338-8570, Japan*
[5]*RIKEN Nishina Center, Wako, Saitama 351-0198, Japan*
[6]*Department of Physics, Niigata University, Niigata 950-2181, Japan*

(Received 12 May 2013; published 16 August 2013)

We measured the reaction cross sections of the two-neutron halo nucleus ^{11}Li with solid hydrogen and carbon targets at around 31 and 41 MeV/nucleon. The neutron density distribution of ^{11}Li was deduced for the first time by the Glauber model calculation based on the optical limit approximation. The uncertainty of the matter density of ^{11}Li was improved, compared with earlier measurements. The present root-mean-square radius of the proton distribution agrees with the previous one derived from an optical isotope shift measurement. The present root-mean-square radii reproduce theoretical calculations by the tensor optimized shell model by assuming core excitation. This consistency suggests the possibility that ^{9}Li in ^{11}Li is excited and the disappearance of the $N = 8$ shell gap of ^{11}Li is caused by correlations originating from the nucleon force, such as the tensor and the pairing.

DOI: 10.1103/PhysRevC.88.024610 PACS number(s): 21.10.Gv, 25.60.Dz, 27.20.+n

I. INTRODUCTION

^{11}Li is known to have a two-neutron halo structure in its ground state. One of the interesting properties of halo nuclei is the large nuclear size due to the dilute density distribution far from the core nucleus, resulting from the small separation energy of one or two valence neutrons. The fact that the interaction nuclear radius of ^{11}Li is larger than those of other lithium isotopes was first reported in Ref. [1]. The quite narrow momentum distribution of ^{9}Li produced through the projectile fragment of ^{11}Li demonstrates a large spatial expansion of two valence neutrons from the uncertainty principle [2]. Since the reaction cross section (σ_R) and the interaction cross section (σ_I) both depend on the incident energy and the kind of target nucleus, these dependencies make it possible to deduce the matter density distributions (ρ_m) of halo nuclei, such as ^{11}Li and ^{11}Be [3,4], with the Glauber model analysis. ρ_m can also be deduced from proton elastic-scattering measurements [5]. These studies show the existence of a long density tail of ^{11}Li.

For studies of unstable nuclei, in particular the physical properties of halo nuclei and the neutron skin thickness, it is valuable to know not only ρ_m but also the proton and neutron density distributions (ρ_p and ρ_n). According to some theoretical studies, the sizes of ρ_p and ρ_n in ^{11}Li depend on whether the core nucleus, ^{9}Li, is excited or not [6–8]. In one experiment, it was found that the root-mean-square (rms) charge radius ($r_{\rm ch}$) of ^{11}Li is larger than that of a bare ^{9}Li from a measurement of the optical isotope shift (OIS) [9]. From these studies, it is important to know ρ_p and ρ_n in ^{11}Li experimentally.

According to the energy dependence of the nucleon-nucleon total cross section ($\sigma_{\rm NN}$) [10], σ_{pn} is about three times larger than σ_{pp} in the low-energy region ($<$100 MeV/nucleon). This property suggests that σ_R for a proton target at these energies is more sensitive to ρ_n than to ρ_p and may allow a good determination of ρ_n by using this sensitivity. Furthermore, σ_R at this low energy is effective for extracting information about the dilute density near the nuclear surface, such as a neutron halo, because of a property that $\sigma_{\rm NN}$ in the low-energy region rapidly increases as the energy decreases. For ^{11}Li, there are few measurements of σ_R in the low-energy region, compared in the high-energy region. In particular, there is only one measurement of σ_R of ^{11}Li on a proton target at an energy of 800 MeV/nucleon [3]. For ^{22}C, σ_R at around 40 MeV/nucleon was measured using a liquid hydrogen target [11], but the determination of ρ_n has never been reported due to a lack of experimental data.

A solid hydrogen target (SHT) is a good tool for the determination of ρ_n. We have already developed a thick and large-area SHT for σ_R measurements [12]. A CH_2 target is also used for σ_R measurements as a proton target because of easy handling but has a statistical disadvantage due to

*Present address: National Cerebral and Cardiovascular Center Research Institute, 5-7-1 Fujishiro-dai, Suita, Osaka 565-8565, Japan.
†Corresponding author: ozawa@tac.tsukuba.ac.jp
‡Present address: Department of Physics and Astronomy, SE-75120 Uppsala, Sweden.
§Present address: Department of Physics, Tokyo University of Science, Noda, Chiba 278-8510, Japan.
∥Present address: Research Center for Electron Photon Science, Tohoku University, Miyagi 982-0826, Japan.
¶Present address: RIKEN Nishina Center, Wako, Saitama 351-0198, Japan.
**Present address: Gesellschaft für Schwerionenforschung GSI, 64291 Darmstadt, Germany.

the subtraction of reaction events with carbon in the CH_2. A SHT has three advantages compared with a liquid one. First, the SHT has a statistical advantage because the density of solid hydrogen is about 20% higher than that of liquid hydrogen. Second, temperature control is not needed for the stable operation of an SHT, while it is necessary for the liquid target to maintain the same density. Third, it is possible to use a thin window, since the operating pressure is much lower than for the liquid target.

The purpose of this study is to deduce an accurate value of ρ_n of ^{11}Li and to present a discussion of this value with current theoretical calculations. For this purpose, we measured σ_R of ^{11}Li on a SHT and a carbon target at energies of around 31 and 41 MeV/nucleon. A measurement of the OIS is an effective method for determining $r_{\rm ch}$ of unstable nuclei precisely, but there are limitations of measurable isotopes due to experimental restrictions, such as low beam intensities, the wavelength of lasers, and ion production. On the other hand, σ_R can be measured within a few percent error even with low beam intensities. It is possible to estimate the rms proton radius (r_p) from the rms neutron radius (r_n) and the rms matter radius (r_m), which are obtained by ρ_n and ρ_m, respectively. If the method to know r_p and r_n only from σ_R measurements is established, it is possible to obtain the neutron skin thickness of unstable nuclei located far from the stability line on the nuclear chart, where the OIS cannot be measured.

II. EXPERIMENT

The experiment was performed using the RIKEN projectile fragment separator (RIPS) [13], a part of the radioactive isotope (RI) beam factory operated by RIKEN Nishina Center and Center for Nuclear Study, the University of Tokyo [14]. A primary beam of ^{18}O was accelerated up to 100 MeV/nucleon in the RIKEN ring cyclotron. A secondary beam was produced by bombardment of the ^{18}O beam on a Be target (10-mm thickness). ^{11}Li particles with energies of 31 and 41 MeV/nucleon were separated by the RIPS. The magnetic rigidity ($B\rho$) of a first dipole magnet before the dispersive focal plane (F1) was adjusted to 4.129 Tm for 31 MeV/nucleon and 4.374 Tm for 41 MeV/nucleon. In F1, a horizontal slit defined the momentum acceptance as $\pm 0.5\%$, and a wedge-shape degrader of 2683 mg/cm^2 Al was installed. The $B\rho$ of a second dipole magnet after F1 was adjusted to 3.672 Tm for 31 MeV/nucleon and 3.607 Tm for 41 MeV/nucleon. The experimental setup around the reaction targets is shown in Fig. 1. The beam position at the reaction target was determined by parallel-plate avalanche counters (PPAC's). Time-of-flight (TOF) between the achromatic focal plane (F2) and the final focal plane (F3) was measured by 0.5-mm-thick plastic scintillators (PL's). The energy loss (ΔE) before the reaction target was measured by a 150-μm-thick silicon detector (Si) placed in F3. After the reaction target, two Si detectors (300-μm thickness each) and a ϕ 5-in. $\times$ 60-mm-thick NaI(Tl) detector were placed in air for measuring ΔE and the total energy (E), respectively. The typical yield and purity of ^{11}Li were 500 cps and 80%, respectively.

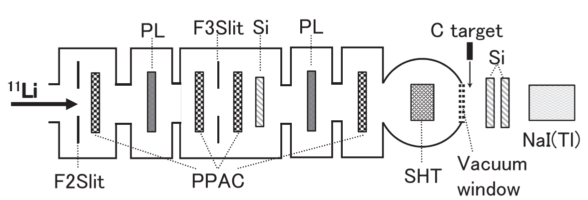

FIG. 1. Schematic view of the experimental setup around reaction targets.

In the present experiment, two reaction targets, a solid hydrogen target (SHT) as a proton target and a carbon target, were used. The volume of the SHT was $\phi\, 50 \times$ 30-mm thickness, corresponding to approximately 0.282 g/cm^2. Kapton foils with 25-μm thickness were used at the entrance and exit windows of the SHT cell. In the case of the measurement with carbon, we installed the carbon target (0.505 g/cm^2) immediately after the vacuum window (a 127-μm-thick Mylar foil) in air with an empty SHT cell. Empty-target measurements were also performed in order to subtract the contribution of reaction events from some detectors.

III. ANALYSIS AND RESULTS

The σ_R value was obtained by the equation $\sigma_R = (-1/N_t) \times \ln(\Gamma/\Gamma_0)$, where Γ is the ratio of the number of noninteracting nuclei to that of incident nuclei for a target-in measurement and Γ_0 is the same ratio for an empty-target measurement. The number of target nuclei per unit area is denoted as N_t. In order to determine the number of incident ^{11}Li (N_1) and that of noninteracting ^{11}Li (N_2), particle identifications (PID's) both before and after the reaction targets were performed.

For the determination of N_1, the PID before the reaction target was performed by the $B\rho$-TOF-ΔE method. Figure 2 shows the TOF-ΔE two-dimensional scattering plot before the reaction target in the measurement using ^{11}Li with an energy of 41 MeV/nucleon. As shown in Fig. 2, ^{11}Li was separated

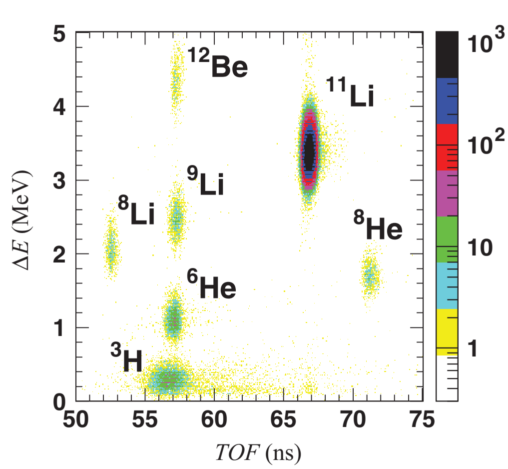

FIG. 2. (Color online) TOF-ΔE two-dimensional scattering plot before the reaction target in the measurement using ^{11}Li with an energy of 41 MeV/nucleon. The intensity is color coded.

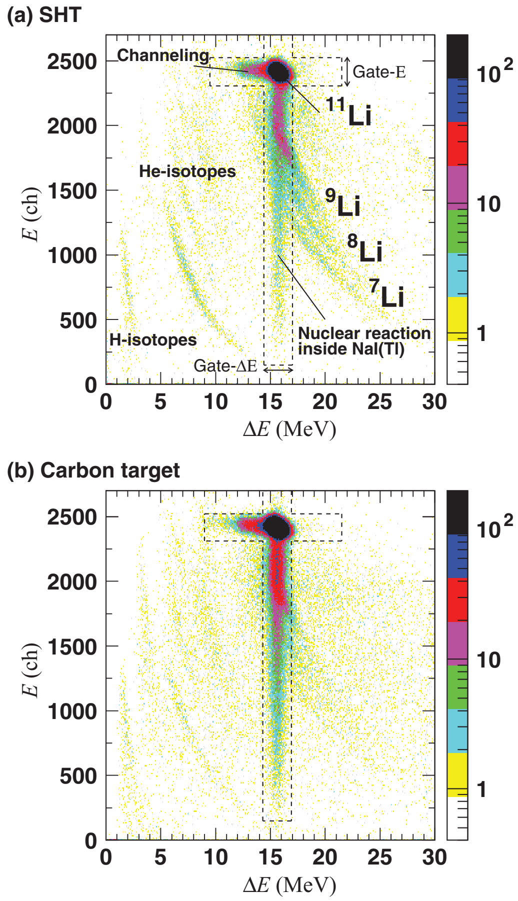

FIG. 3. (Color online) ΔE-E two-dimensional scattering plots after (a) the SHT and (b) the carbon target in the measurement using ^{11}Li at around 41 MeV/nucleon, where ^{11}Li is selected before the reaction targets. The broken lines are the gates that are established for counting the noninteracting ^{11}Li. The intensity is color coded.

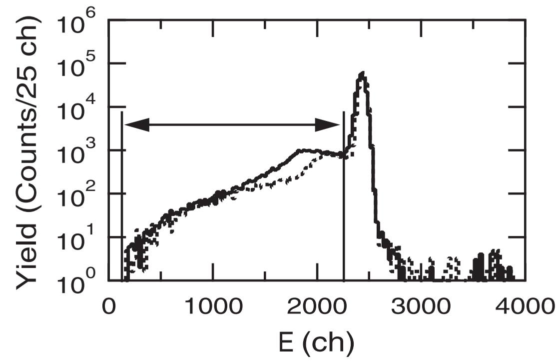

FIG. 4. E distribution of the particles selected by the gate shown in Fig. 3(a). The solid and dotted lines indicate the E distributions in the case of experiments using the SHT and empty target, respectively. The arrow indicates the range of the subtraction to obtain the number of Li isotopes, which are located inside the gate.

sufficiently from other nuclei. In order to determine N_1, a least-squares method with a Gaussian function was applied to the TOF axis and the ΔE axis after ^{11}Li fragments were projected to both axes. ^{11}Li fragments, which are in the range of ± 1 sigma of each axis, were determined as N_1 in the present analysis.

For the determination of N_2, the PID after the reaction target was performed by the ΔE-E method. Figures 3(a) and 3(b) show ΔE-E two-dimensional scattering plots after the SHT and the carbon target, respectively, where ^{11}Li was selected before the reaction targets. The main peak shown in Fig. 3 indicates the noninteracting ^{11}Li with each reaction target. Two tails from the main peak toward the low ΔE and the low E are produced by channeling in the Si detectors located downstream of the reaction targets and the nuclear reaction inside NaI(Tl), respectively. These events should be counted as N_2. Li isotopes are produced by neutron removal reactions of ^{11}Li with each reaction target.

In order to count the noninteracting ^{11}Li precisely, we established the gates indicated by the broken lines in Fig. 3. Both widths of the gate, which are indicated by "Gate-ΔE" and "Gate-E," correspond to six sigma obtained by Gaussian fitting to the main peak projected to the ΔE axis and the E axis, respectively. In order to eliminate a part of the Li isotopes located in the gate, we used the data of the empty-target measurements. Figure 4 shows the E distributions of particles selected by the gate shown in Fig. 3(a) compared with that of the empty-target measurement. The number of incident particles into NaI(Tl) in the empty-target measurement shown in Fig. 4 was normalized to that of the SHT measurement. We assumed that the response functions of NaI(Tl) are approximately the same between both measurements because the incident energy of ^{11}Li in the empty-target measurement was adjusted to match that of the SHT measurement. Using this assumption, it was possible to estimate the number of Li isotopes located in the gate as the difference between both E distributions shown in Fig. 4. N_2 was determined by subtracting the number of the estimated Li isotopes from the number of all particles in the gate. Carbon target and empty-target measurements were applied to the same analysis mentioned above.

The thickness of the SHT depends on the position of incident particles, because the surfaces of the SHT swell due to thin entrance and exit windows. We have determined that the surface of the SHT can be approximated by a second-order polynomial function [12]. In the present study, we used the effective thickness as N_t, which is considering the statistical weight depending on the beam position of ^{11}Li entering into the entrance of the SHT.

In carbon target measurements, an inelastic scattering with carbon is one of the important reaction channels. As shown in Fig. 3(b), there are no inelastic-scattering events. Furthermore, bound excited states of ^{11}Li have not been reported yet. Thus, the inelastic scattering of ^{11}Li with a carbon target was neglected in the present analysis.

The reaction cross sections obtained in the present study are summarized in Table I together with earlier data. Note that σ_I in the high-energy region are approximated to σ_R [15]. The experimental error of σ_R takes into account the statistical error, uncertainties of the target thickness, and error due to the estimation of Li isotopes.

TABLE I. Summary of experimental σ_R of ^{11}Li. The energies for the data obtained by this work are given for the middle of the reaction targets.

Energy (MeV/nucleon)	σ_R (mb)	References
	Proton target	
31	774 ± 18	Present work
41	685 ± 17	Present work
800	276 ± 8	[3]
	Carbon target	
31	1938 ± 70	Present work
40	1774 ± 45	Present work
45	1740 ± 30	[16]
87	1260 ± 40	[17]
400	989 ± 21	[3]
790	1047 ± 40	[18]

IV. DISCUSSION

A. Glauber model calculations

We compared the experimental results with Glauber model calculations. There are different kinds of the Glauber model, such as the few-body treatment [19] and a model taking into account the Fermi motion effect [20]. We used the optical limit approximation (OLA) [21], as used in earlier studies [3,4], and applied the finite-range treatment in the present study [22–24]. With the OLA, σ_R can be calculated by integrating the projectile and target densities within their overlap region. In Glauber model calculations, it is necessary to assume density functions with some free parameters. For ρ_p of ^{11}Li, we assumed a Gaussian shape. For ρ_n of ^{11}Li, we assumed a Gaussian shape with a Yukawa-square tail, which is known to be a good approximation to the shape of a single-particle density at the outer region of a core with centrifugal barriers. These functions are expressed as follows:

Matter density

$$\rho_m(r) = \rho_p(r) + \rho_n(r), \tag{1a}$$

Proton density

$$\rho_p(r) = X_p \exp\left[-\left(\frac{r}{a_p}\right)^2\right], \tag{1b}$$

Neutron density

$$\rho_n(r) = X_n \exp\left[-\left(\frac{r}{a_n}\right)^2\right] (r \leqslant r_c), \tag{1c}$$

$$\rho_n(r) = Y_n \frac{\exp[-\lambda r]}{r^2} (r > r_c), \tag{1d}$$

where a_p, a_n, and λ are the width parameters of ρ_p and ρ_n and the slope of the tail, respectively; r_c is the point where the Gaussian and the Yukawa tail intersect. The amplitude (X_p, X_n, Y_n) of each distribution is normalized by the proton and neutron numbers of ^{11}Li, which are equal to 3 and 8, respectively. ρ_m is represented by the sum of ρ_p and ρ_n, as shown in Eq. (1a). The free parameters [a_p, a_n, λ, (X_n/Y_n)] were determined by χ^2 fitting so as to reproduce the experimental results listed in Table I. Figure 5 shows the energy dependence of σ_R of ^{11}Li on proton and carbon targets. The solid lines in Fig. 5 indicate the best-fit curves.

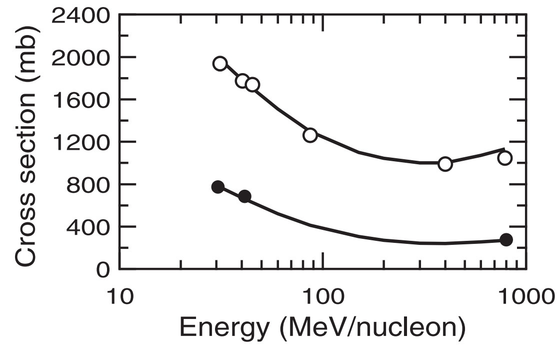

FIG. 5. Energy dependence of σ_R of ^{11}Li. Closed and open circles denote experimental data using a proton target and a carbon target, respectively. Solid lines are best-fit curves.

B. Density distributions

Figure 6 shows the density distributions of ^{11}Li obtained by the best-fit parameters. Bands of these densities, which were obtained by varying free-parameter sets within the

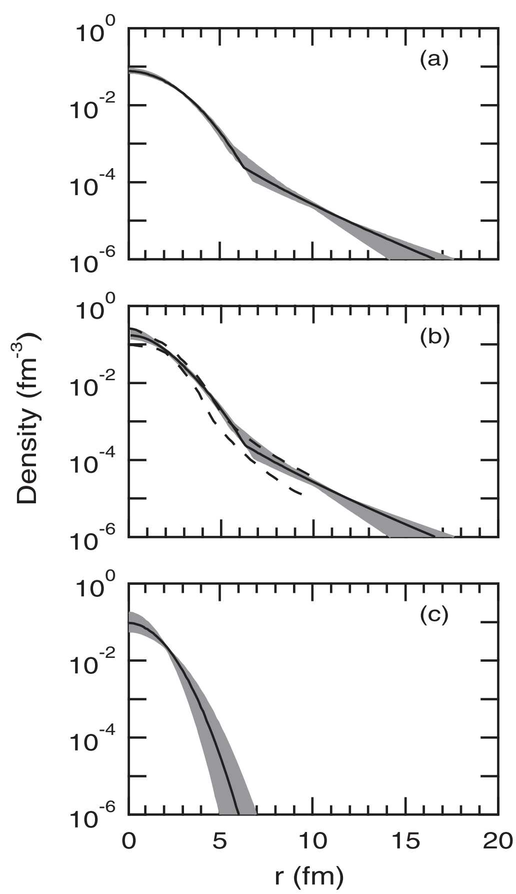

FIG. 6. Density distributions of ^{11}Li: (a) ρ_n, (b) ρ_m, and (c) ρ_p. Best-fit densities are indicated by the thick solid curves, and uncertainties are shown by shaded regions. The dashed lines indicate the upper and lower limits of ρ_m deduced by the σ_I experiment [3].

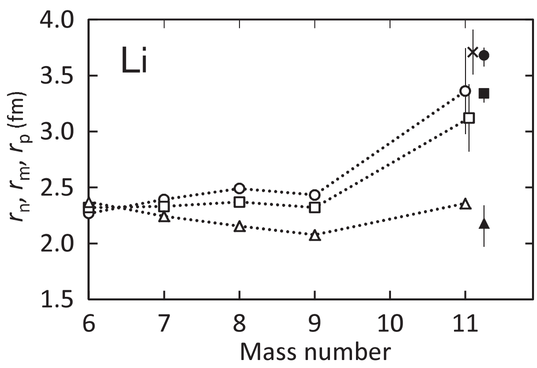

FIG. 7. Root-mean-square (rms) neutron (r_n), matter (r_m), and proton (r_p) radii of Li isotopes obtained from experimental studies. The circles, squares, and triangles are r_n, r_m, and r_p, respectively. The closed symbols indicate present experimental results. The error bar of present r_p indicates the uncertainty obtained by the method using present r_n and r_m with Eq. (2). The open circles indicate previous r_n obtained from r_m and r_p with Eq. (2). The open squares indicate previous r_m determined by the σ_I experiment [3,18]. The cross symbol indicates the previous r_m determined by the proton elastic-scattering measurement [5]. The open triangles indicate previous r_p converted from the rms charge radii obtained by the OIS measurement with Eq. (3) except for that of ^{7}Li, which was determined by the electron scattering [9].

uncertainties of each free parameter, are represented as uncertainties of densities. As shown in Fig. 6(a), it was possible to deduce ρ_n experimentally for the first time in the present study. We compared the present ρ_m with that of an earlier σ_I experiment [3], as shown in Fig. 6(b). The previous ρ_m was deduced by the Glauber model calculation so as to reproduce σ_I on a proton, a deuteron, a carbon, and a beryllium target at energies of 400 and 800 MeV/nucleon. As shown in Fig. 6(b), the present ρ_m reproduces the previous one. The improvement of the uncertainty in the present study is likely to be due to the χ^2 fitting using the energy dependence of σ_R in the low- and high-energy regions. Figure 6(c) shows the present ρ_p of ^{11}Li. The uncertainty of ρ_p is larger than that of ρ_n. The reason for this is that σ_R on a proton target is more sensitive to a neutron density distribution of a projectile than that of a proton density from properties of $\sigma_{\rm NN}$ in the low-energy region, as mentioned in the introduction.

C. Root-mean-square radii

Figure 7 shows the root-mean-square (rms) neutron (r_n), matter (r_m), and proton (r_p) radii of Li isotopes in the present and earlier experimental studies. Table II is a summary of the experimental rms radii of Li isotopes. The present r_n and r_m were obtained from ρ_n and ρ_m shown in Fig. 6, respectively, while the present r_p was obtained by using two different methods. One is the method using ρ_p shown in Fig. 6(c), the same as the methods applied to the present r_n and r_m. The other is a method using the present r_n and r_m with the following relation:

$$r_m^2 = \left(\frac{Z}{A}\right) r_p^2 + \left(\frac{N}{A}\right) r_n^2. \tag{2}$$

In this case, the error of r_p was estimated by the error propagation, taking into account the covariance due to the correlation between r_n and r_m. The previous r_p was converted from the rms charge radius ($r_{\rm ch}$), which was deduced precisely from the optical isotope shift (OIS) measurement [9], by using the following equation:

$$r_p^2 = r_{\rm ch}^2 - \langle R_p^2 \rangle - \frac{N}{Z}\langle R_n^2 \rangle - \frac{3\hbar^2}{4m_p^2c^2}, \tag{3}$$

where $\langle R_p^2 \rangle$ and $\langle R_n^2 \rangle$ are the proton [25] and neutron [26] rms charge radii, respectively. The last term on the right-hand side indicates the Darwin-Foldy correction [27]. As shown in Fig. 7, it is found that r_m of ^{11}Li is larger than those of other Li isotopes because ^{11}Li has a halo structure. The tendency of r_n between Li isotopes is similar to that of r_m. The reason for this is that the second term on the right-hand side of Eq. (2) is dominant for r_m of neutron-rich nuclei. As reported in Ref. [9], r_p of ^{11}Li is larger than that of ^{9}Li. This enhancement of ^{11}Li is thought to be due to the correlated relative motion between the core nucleus and the two valence neutrons. In the present study, r_n, r_m, and r_p of ^{11}Li can be derived only from σ_R measurements.

Figure 8 shows rms radii of ^{11}Li. Figure 8(a) shows results of r_n. It is necessary to know r_m and r_p in the conventional method for the derivation of r_n. In the present study, it was possible to obtain r_n from ρ_n without Eq. (2). In Fig. 8(b), the present r_m agrees with that previously deduced using only the previous σ_I data [3]. The improvement of the uncertainty

TABLE II. Experimental results of root-mean-square (rms) nuetron (r_n), matter (r_m), and proton (r_p) radii of Li isotopes. The previous r_n were obtained from the previous r_m and r_p with Eq. (2). The previous r_p were converted from the rms charge radii ($r_{\rm ch}$) with Eq. (3).

		r_n	r_m	$r_{\rm ch}$ [9]	r_p
Previous work	^{6}Li	2.27 ± 0.07	2.32 ± 0.03 [18]	2.517 ± 0.030	2.370 ± 0.032
	^{7}Li	2.39 ± 0.04	2.33 ± 0.02 [18]	2.39 ± 0.03	2.24 ± 0.03
	^{8}Li	2.49 ± 0.04	2.37 ± 0.02 [18]	2.299 ± 0.032	2.155 ± 0.034
	^{9}Li	2.43 ± 0.03	2.32 ± 0.02 [18]	2.217 ± 0.035	2.076 ± 0.037
	^{11}Li	3.36 ± 0.38	3.12 ± 0.30 [3]	2.467 ± 0.037	2.358 ± 0.039
			3.71 ± 0.20 [5]		
Present work	^{11}Li	$3.68^{+0.07}_{-0.10}$	$3.34^{+0.04}_{-0.08}$		$2.18^{+0.16}_{-0.21}$ [a]
					2.18 ± 0.40 [b]

[a]The method using the present r_n and r_m with Eq. (2).
[b]The method using the present ρ_p.

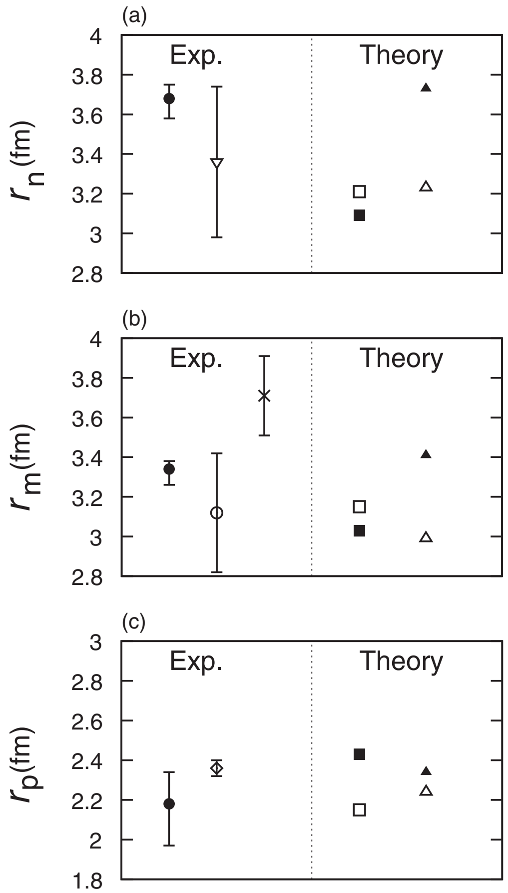

FIG. 8. Root-mean-square (rms) neutron (r_n), matter (r_m), and proton (r_p) radii of ^{11}Li. The closed circles indicate the present experimental results. The error bar of present r_p indicates the uncertainty obtained by the method using present r_n and r_m with Eq. (2). The open circle and the cross symbol indicate the previous r_m from the σ_I measurement [3] and the proton elastic-scattering measurement [5], respectively. The diamond symbol indicates the previous r_p, which is converted from the rms charge radius obtained by the OIS measurement [9]. The open inverse triangle indicates the previous r_n obtained from the previous r_m reported in Ref. [3] and the previous r_p with Eq. (2). The open and closed squares indicate the theoretical calculations by SVMC [6,7] assuming an inert core and excited core, respectively. The open and closed triangles are the same as the squares, but for the theoretical calculations by TOSM [8].

of the present r_m means that the present ρ_m is more accurate than the previous one, because the outer region of the nuclear surface of ^{11}Li was investigated in a better way by using σ_R in the low-energy region. The previous r_m, obtained from a proton elastic-scattering experiment [5], is larger than those of the present study and the σ_I measurement. According to Ref. [5], r_m depends on the value of the one-neutron separation energy which is included as the input parameter in the density function of the tail assumed in the previous analysis, and the large error of r_m is mainly due to the uncertainty of the radius where the core density intersects with part of the tail. Figure 8(c) shows results of r_p. As shown in Table II, there are no differences between the mean values of the present r_p obtained by using the two methods mentioned above. However,

TABLE III. Theoretical results of rms radii of ^{11}Li calculated by SVMC [6,7] and TOSM [8].

	r_n	r_m	r_p
	SVMC		
Inert core	3.21	3.15	2.15
Excited core	3.09	3.03	2.43
	TOSM		
Inert core	3.23	2.99	2.24
Excited core	3.73	3.41	2.34

the error of r_p in the case using r_n and r_m with Eq. (2) is less than that of the other case. This result demonstrates that in the present study it was easier to deduce ρ_n and ρ_m than ρ_p. The present r_p agrees within the experimental uncertainty with the previous r_p, which was converted from r_{ch} [9]. This result demonstrates that in the present study it was possible to deduce r_p experimentally by only using σ_R measurements. The large error of the present r_p is considered to be the poor sensitivity of the proton density of a projectile to a proton target, which is derived from the property of the σ_{NN}.

The deduced rms radii of ^{11}Li were compared with two theoretical calculations, as shown in Fig. 8. One is the stochastic variational multicluster (SVMC) [6,7], which is a microscopic cluster model assumed by α-, triton-, and single-neutron clusters in order to include the free degree of the distortion in the core nucleus ^{9}Li. The other is the tensor optimized shell model (TOSM) [8], which makes it possible to indicate that the s-p shell gap for ^{11}Li becomes small due to the tensor and pairing correlations created by the configuration mixing of the particle-hole pair. Table III shows theoretical results of the rms of ^{11}Li calculated by SVMC and TOSM. While there are many theoretical calculations for ^{11}Li, the above two models have a feature that the physical quantities of ^{11}Li are calculated by assuming two cases whether the core nucleus ^{9}Li is excited or not (core excitation and distortion are synonymous in this case). As shown in Fig. 8(c), both models predict an enhancement of r_p in the case of core excitation. However, predictions of r_n and r_m in the case of core excitation are opposite tendencies in both models, as shown in Figs. 8(a) and 8(b). According to the authors in Ref. [7], the small r_m calculated by SVMC in the case of core excitation is due to the large two-neutron separation energy, which is about 200 keV larger than that of the other case. In TOSM, the enhancement of r_m in the case of core excitation is due to the large s-wave probability. As shown in Fig. 8, r_n, r_m, and r_p obtained from the present study are consistent with each result calculated by TOSM in the case of core excitation. From these consistencies, it might be that the shell model is more suitable for the picture of ^{11}Li than the cluster model. Taking into account the excitation of ^{9}Li with TOSM, T. Myo *et al.* [8] found that configuration mixings of $(0p_{3/2})^{-2}(0p_{1/2})^2$ and $(0s)^{-2}(0p_{1/2})^2$ are enhanced by the pairing correlation and the tensor correlation in ^{9}Li, respectively. Since the 2p-2h excitations in ^{9}Li are Pauli blocked by two additional neutrons in the $0p_{1/2}$ orbit, the p shell was pushed up in energy so as to narrow the s-p shell gap. This blocking effect produces the increasing of the s^2 component of valence neutrons and the enhancement of the nuclear size. Although further studies are necessary in order to obtain a deeper understanding of the behavior of ^{11}Li, the consistency of the present rms radii of ^{11}Li with the results of TOSM suggests the possibility that ^{9}Li in ^{11}Li is excited, and the disappearance of the $N = 8$ shell gap in ^{11}Li is caused by correlations originating from the nucleon force, such as the tensor and the pairing.

V. SUMMARY

We measured σ_R of ^{11}Li with solid hydrogen and carbon targets at around 31 and 41 MeV/nucleon. The neutron density distributions of ^{11}Li were deduced well by the Glauber model analysis based on the optical limit approximation, which reproduces the energy dependence of the present and earlier experimental data. The uncertainty of the matter density of ^{11}Li was improved, compared with the previous one. The present root-mean-square proton radius agrees with the previous one derived from the optical isotope shift measurement. This result demonstrates that it is possible that the skin thickness of unstable nuclei, which is located far from the stability line on the nuclear chart, can be obtained experimentally by only using σ_R measurements without optical isotope shift measurements. The root-mean-square radii of ^{11}Li obtained in the present study reproduce theoretical results calculated by the tensor optimized shell model assuming core excitation. This consistency supports the possibility that ^{9}Li in ^{11}Li is excited and the disappearance of the $N = 8$ shell gap of ^{11}Li is caused by correlations originating from the nucleon force such as the tensor and the pairing.

ACKNOWLEDGMENTS

The authors thank the members of the RIKEN accelerator staff for stable operation of the accelerators and related devices. T.M. also thanks the junior research associate program at RIKEN.

[1] I. Tanihata *et al.*, Phys. Rev. Lett. **55**, 2676 (1985).
[2] T. Kobayashi *et al.*, Phys. Rev. Lett. **60**, 2599 (1988).
[3] I. Tanihata *et al.*, Phys. Lett. B **287**, 307 (1992).
[4] M. Fukuda *et al.*, Phys. Lett. B **268**, 339 (1991).
[5] A. V. Dobrovolsky *et al.*, Nucl. Phys. A **766**, 1 (2006).
[6] Y. Suzuki, R. G. Lovas, and K. Varga, Prog. Theor. Phys. Suppl. **146**, 413 (2002).
[7] K. Varga, Y. Suzuki, and R. G. Lovas, Phys. Rev. C **66**, 041302 (2002).
[8] T. Myo, Y. Kikuchi, K. Katō, H. Toki, and K. Ikeda, Prog. Theor. Phys. **119**, 561 (2008).
[9] R. Sánchez *et al.*, Phys. Rev. Lett. **96**, 033002 (2006).
[10] Paticle data group, http://pdg.lbl.gov/xsect/contents.html.
[11] K. Tanaka *et al.*, Phys. Rev. Lett. **104**, 062701 (2010).
[12] T. Moriguchi *et al.*, Nucl. Instrum. Methods Phys. Res. A **624**, 27 (2010).
[13] T. Kubo *et al.*, Nucl. Instrum. Methods Phys. Res. B **70**, 309 (1992).
[14] Y. Yano, Nucl. Instrum. Methods Phys. Res. B **261**, 1009 (2007).
[15] A. Ozawa *et al.*, Nucl. Phys. A **709**, 60 (2002).
[16] N. Inabe *et al.*, RIKEN Accel. Prog. Rep. **24**, 9 (1991).
[17] B. Blank *et al.*, Nucl. Phys. A **555**, 408 (1993).
[18] I. Tanihata *et al.*, Phys. Lett. B **206**, 592 (1988).
[19] Y. Ogawa, K. Yabana, and Y. Suzuki, Nucl. Phys. A **543**, 722 (1992).
[20] M. Takechi *et al.*, Phys. Rev. C **79**, 061601 (2009).
[21] P. J. Karol, Phys. Rev. C **11**, 1203 (1975).
[22] T. Zheng *et al.*, Nucl. Phys. A **709**, 103 (2002).
[23] D. Q. Fang *et al.*, Phys. Rev. C **69**, 034613 (2004).
[24] C. Wu *et al.*, Nucl. Phys. A **739**, 3 (2004).
[25] I. Sick, Phys. Lett. B **576**, 62 (2003).
[26] S. Kopecky *et al.*, Phys. Rev. C **56**, 2229 (1997).
[27] J. L. Friar, J. Martorell, and D. W. L. Sprung, Phys. Rev. A **56**, 4579 (1997).